

# Energy-efficient active integrated photonic isolators using electrically driven acoustic waves

Nathan Dostart<sup>1,\*</sup>, Yossef Ehrlichman<sup>1</sup>, Cale Gentry<sup>1</sup>, and Miloš Popović<sup>2</sup>

<sup>1</sup>Department of Electrical, Computer, and Energy Engineering, University of Colorado, Boulder, CO, 80309, USA

<sup>2</sup>Department of Electrical and Computer Engineering, Boston University, Boston, MA, 02215, USA

\*Corresponding author: nathan.dostart@colorado.edu

Compiled November 6, 2018

## Abstract

We propose and investigate the performance of integrated photonic isolators based on a triply-guided waveguide system on chip comprising two optical modes and an electrically-driven acoustic mode. One optical mode carries a signal of interest; the second is ancillary and takes away optical power rejected by the isolator. The acoustic wave induces linear optical non-reciprocity with no additional optical loss, without magnetic-optic materials, and with low power consumption. These properties suggest the potential for straightforward integration with the drive circuitry, possibly in monolithic CMOS technology, enabling a fully contained ‘black box’ optical isolator with two optical ports and DC electrical power. The approach is theoretically evaluated using realistic parameters; our example implementation includes a novel optical-mechanical multiplexer design. Expected performance is a predicted 20 dB of isolation and 3.5 dB of insertion loss with 380 GHz optical bandwidth and a 1 cm device length. The isolator utilizes 1 mW of electrical drive power, or 10 fJ/bit at the 100 Gbps equivalent data rate supported by the isolator, an improvement of 1 – 3 orders of magnitude over the state-of-the-art. Such isolators could be valuable in integrated photonic communication and sensing circuits, especially those using coherent detection.

Integrated photonics is rapidly advancing and will become an integral part of future computing and communication technologies, including through co-integration of state-of-the-art electronics and silicon photonics [1]. Many integrated photonics applications call for co-integration with on-chip lasers, which require optical isolators. Even for architectures that use off-chip lasers, on-chip isolators or circulators could enable simultaneous bi-directional communication links and other capabilities. Conventional isolators use the magneto-optic (Faraday) effect to induce non-reciprocity, but magneto-optic materials have substantial loss and have been challenging to integrate in photonic platforms [2, 3, 4, 5]. To our knowledge, no silicon photonics foundry currently has an optical isolator in its component library. In contrast, monolithic co-integration of electronics and photonics has been demonstrated in advanced process nodes (28 – 45 nm) [6, 1]. Hence, non-magnetic approaches to integrated photonic isolation, preferably CMOS-compatible, are desirable and would be rapidly adopted.

Aside from the magneto-optic effect, two other avenues exist to produce a non-reciprocal system: nonlinearity and time variance [7]. Signal-nonlinear approaches cannot be used for many applications, but some nonlinear approaches based on stimulated Brillouin scattering (SBS) are signal-linear [8, 9]. However, these approaches require two optical pumps, which combined with typical laser wall plug efficiencies of  $\sim 10\%$  and high required pump power cause this to be a power hungry and expensive prospective approach. Time-varying systems, mostly based on optoelectronic interactions, are the basis for a wide array of proposed isolator designs using effects such as frequency conversion, traveling wave phase shifters, and optical interband transitions [10, 11, 12, 13]. The main drawback of current silicon photonic approaches is free carrier loss inherent to plasma-dispersion modulators [14] and their typically low isolation ratios of  $< 15$  dB [11, 13, 10].

In this Letter we investigate integrated photonic isolators that utilize an optical guided wave ‘interband transition’ i.e. mode conversion [12] facilitated by non-reciprocal coupling induced by an electronically excited traveling guided acoustic wave. We refer to them as electro-mechanical photonic (EMP) isolators. This approach avoids the requirement of two optical pumps [8, 9], achieves lower insertion losses and higher isolation than carrier plasma approaches [13, 11, 10], and may use potentially co-integrated electronics to generate the acoustic wave to result in a self-contained device. A recent paper demonstrates a similar isolation approach in an optical resonator with an unconfined, standing acoustic wave [15]. Our design uses a co-propagating, guided acoustic wave in a velocity-matched optical/acoustic waveguide to achieve broader bandwidth and higher energy efficiency.

The key components of the EMP isolator are a triply-guiding (bi-optical, uni-acoustic) waveguide cross-section with strong optomechanical coupling and tailored dispersion, and a novel ‘acoustic injector’ which multiplexes the optical modes with a transduced acoustic mode. We assume a piezoelectric transducer for maximum transduction efficiency since low-loss

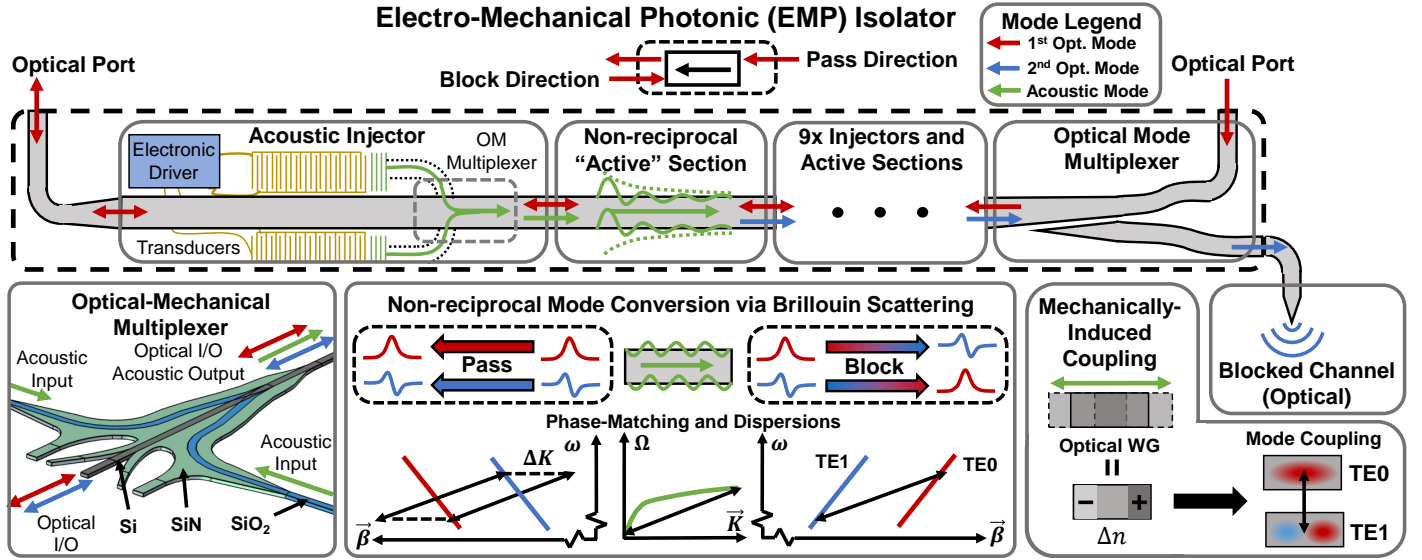


Figure 1: Schematic of EMP isolator with components and operating principles. An ‘acoustic injector’ combines an electrically-transduced acoustic mode with the optical modes in an optical-mechanical multiplexer which provides the input to an ‘active’ section. This active section facilitates optical mode conversion in the block direction, but not in the pass direction, using the acoustic wave. The acoustic decay is compensated by multiple acoustic injectors, each followed by a corresponding active section, to provide the required non-reciprocity. Following the non-reciprocal section, the modes are split apart by a mode multiplexer and the second optical mode leaves the isolator irreversibly (shown here as a radiative taper). Insets: (bottom-left) optical-mechanical multiplexer structure and ports, (bottom-center) non-reciprocal mode conversion, dispersions, and phase-matching in the active section, and (bottom-right) pictorial representation of the optomechanical coupling.

piezoelectrics have been co-integrated with CMOS photonics [16]. However, use of non-piezoelectric CMOS transducers, previously demonstrated [17], could enable entirely monolithic (and ‘zero-change’ [1]) CMOS photonic isolators.

The operating principle and a schematic of one embodiment are shown in Fig. 1. We use a non-reciprocal ‘interband’ (mode-to-mode) transition [12], where conversion from one optical spatial mode to another occurs in one direction but not in the other due to direction-dependent phase-matching. We then spatially separate these two modes using an adiabatic mode multiplexer. The converted power is discarded for an isolator (or retained for a circulator).

The non-reciprocal interband transition is provided by a linear optomechanical interaction. As shown in Fig. 1, a traveling acoustic wave is launched by a transducer into an ‘active’ optomechanical waveguide via an ‘acoustic injector’, which unidirectionally injects the acoustic wave into the optomechanical waveguide without affecting the optical modes. The optomechanical waveguide co-confines both light and sound such that the acoustic mode couples the incident optical mode and a second optical mode via Brillouin scattering [18]. The active section converts all power in one optical mode to the second mode in the ‘block’ direction of the isolator but no power in the ‘pass’ direction. This implementation uses a forward Brillouin interaction, where the optical modes are co-propagating, to maximize the optical bandwidth. A backwards Brillouin interaction, while allowing for shorter device length, constrains the optical bandwidth to approximately the acoustic frequency.

We use the coupled mode theory treatment of optomechanical interactions in [18]. The optical and acoustic fields are represented in their respective modal bases,  $\vec{E} = A_1(z)\vec{\mathcal{E}}_1(x, y)e^{j(\omega_1 t - \beta_1 z)} + A_2(z)\vec{\mathcal{E}}_2(x, y)e^{j(\omega_2 t - \beta_2 z)}$ ,  $\vec{u} = B(z)\vec{U}(x, y)e^{j(\Omega t - Kz)}$ . Here  $\vec{E}$  and  $\vec{u}$  represent the total electric field and acoustic displacement field;  $\vec{\mathcal{E}}_i$  and  $\vec{U}$  are the modal field shapes;  $\omega_i$  and  $\Omega$  are the mode frequencies;  $\beta_i$  and  $K$  are the modal propagation constants; and  $A_i$  and  $B$  denote the wave amplitudes (the modal shapes are normalized such that the powers are given by  $|A_i|^2$ ,  $|B|^2$ ).

The coupled mode equations that describe interactions between these modes are [18]

$$\frac{\partial A_1}{\partial z} = j\omega_1\kappa_{12}B^*e^{j\Delta Kz}A_2 - \alpha_{opt}A_1 \quad (1)$$

$$\frac{\partial A_2}{\partial z} = j\omega_2\kappa_{21}Be^{-j\Delta Kz}A_1 - \alpha_{opt}A_2 \quad (2)$$

$$B = B_0e^{-\alpha_{acst}z} \quad (3)$$

where  $\kappa_{ij}$  denotes the optomechanical coupling between mode  $i$  and mode  $j$  induced by the presence of the acoustic wave,  $\Delta K = K - (\beta_1 - \beta_2)$  is the wave-vector mismatch of the interaction,  $\alpha_{opt}$  is the optical propagation loss rate, and  $\alpha_{acst}$  is the

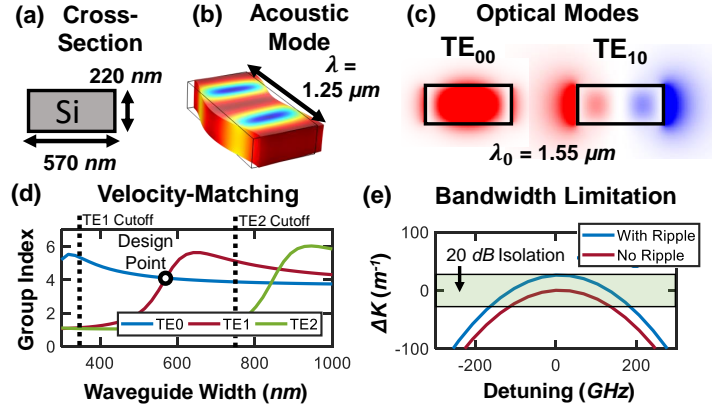


Figure 2: EMP isolator design parameters: (a) active region cross-section, (b) acoustic mode, and (c) optical modes. (d) Group index of the first three TE modes vs. waveguide width, and design width. (e) Wave-vector mismatch with detuning and acceptable mismatch for 20 dB isolation.

acoustic propagation loss rate. The optomechanical coupling  $\kappa_{ij}$  between the two optical modes is principally induced by the photoelastic effect and the moving boundary effect. Through field symmetries  $\kappa \equiv \kappa_{ij} = \kappa_{ji}^*$  [18]. We neglect terms which involve optical pumping of the acoustic wave because we assume that *the acoustic wave is an ‘undepleted pump’*. Brillouin scattering requires one phonon per converted photon, hence to convert  $P_{opt} = 1$  mW of optical power between two optical modes with a 10 GHz acoustic wave, only  $(\Omega/\omega)P_{opt} = 5$  nW of acoustic power is required. Thus, for acoustic guided power of  $\geq 1$   $\mu$ W, this assumption is justified.

For simplicity, we define an effective optical coupling  $\bar{\kappa} \equiv |\kappa||B_0|\sqrt{\omega_1\omega_2}$ , analogous to the coupling coefficient used in standard optical waveguide coupled mode theory [19]. We then find the lossless coupling length (at which all power is mode-converted in the absence of acoustic loss and with perfect phase-matching) as  $l_c^0 = \pi/(2\bar{\kappa})$ . Strong mechanical coupling between the two optical modes ( $\kappa$ ) and efficient excitation of the acoustic wave ( $|B_0|$ ) are therefore essential for a short device length. We can tune the strength and phase of the effective optical coupling *in situ* via the acoustic power and phase. In the presence of high acoustic propagation loss, the optical coupling decays with the acoustic wave, which can be compensated by re-injecting acoustic power periodically along the waveguide.

The phase-matching condition for forward Brillouin scattering determines the needed acoustic wave-vector  $K = \beta_1 - \beta_2$  and acoustic frequency  $\Omega = \omega_1 - \omega_2$ . The second optical mode starts out unexcited at the entrance to the structure and is automatically built up along the waveguide at the energy-matched frequency in steady-state operation. Correct phase-matching in the block direction provides mode conversion, and lack of phase-matching in the pass direction suppresses it, providing the non-reciprocity. The effect of phase-mismatch can be evaluated by solving Eqs. (1–2) (without loss) for the output amplitudes, with the primary effect being a shorter coupling length  $l'_c = (\pi/2)(\bar{\kappa}^2 + \Delta K^2/4)^{-1/2}$ .

For the proposed device, the achievable wave-vector mismatch in the pass direction (given a requirement of phase-matching in the block direction) sets the minimum device length. To design a short device we need to maximize the coupling coefficient  $\bar{\kappa}$  for a given  $\Delta K$ . Power conversion occurs with a shorter cycle period (length) in the presence of phase-mismatch [19]. We can use this to achieve full isolation by choosing the device length  $L$  to correspond to a null of the sinusoidal conversion in the phase-mismatched direction ( $L = 2l'_c$ ) and a peak of the conversion in the phase-matched direction ( $L = l_c^0$ ). Assuming the bandwidth-maximizing scenario of identical optical group indices for the two optical modes (described later), the phase-mismatch is a function only of the acoustic frequency and optical group index,  $\Delta K = 2\Omega n_g/c$ . Using this relation we see that the device length required for full isolation is fully determined by these two parameters:

$$L = \frac{\pi\sqrt{3}}{2} \frac{1}{\Omega} \frac{c}{n_g}. \quad (4)$$

A shorter device requires increasing the acoustic frequency or decreasing the optical group velocity (e.g. slow light).

Next we evaluate the device’s performance for an example implementation, by numerically solving Eqs. (1–3). We choose a standard silicon thickness of 220 nm and assume some device parameters necessary to calculate the isolator performance based on previously fabricated device literature. We assume a piezoelectric transducer with efficiency of  $-14$  dB [15], an acoustic loss rate of  $\alpha_{acst} = 1$  mm $^{-1}$  (87 dB/cm) [20], and an optical loss rate of  $\alpha_{opt} = 2.4$  dB/cm [21]. For the optical mode multiplexer in 220 nm SOI we use  $-30$  dB crosstalk and  $\sim 1$  dB of insertion loss over a  $\sim 2$  THz bandwidth as demonstrated in adiabatic couplers [22].

The example active region, interacting modes, and phase-matching considerations are shown in Fig. 2. For the active section geometry we consider a suspended beam [Fig. 2(a)]. For the optomechanical interaction, a horizontal shear wave [Fig. 2(b)] is used to couple the first and second TE optical modes [Fig. 2(c)]. For this configuration the optimal beam width is 570 nm at which the two optical modes have *identical* group indices of  $n_g = 4.11$  [Fig. 2(d)]. We match group velocities to

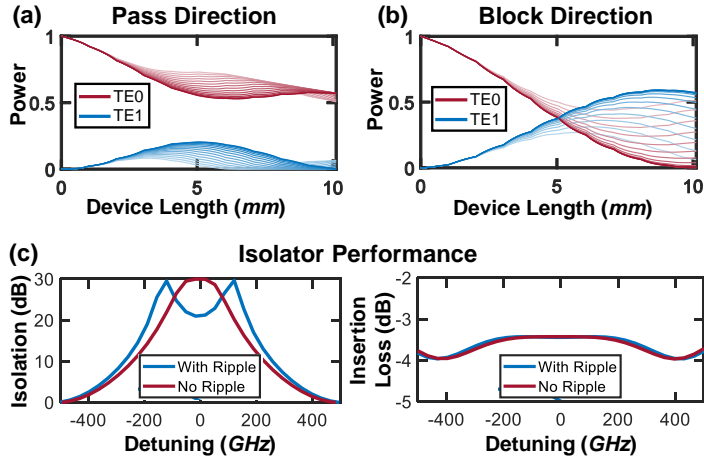


Figure 3: Simulated modal power conversion in (a) pass and (b) block directions including loss and dispersion. Detuning from center wavelength is shown in lighter shades in 30 GHz increments up to 480 GHz. (c) Device performance including effects of the mode multiplexer, with and without the bandwidth-maximizing ripple.

Parameter	Kittlaus [9]	Sohn [15]	Poulton [8]	Dong [11]	Lira [13]	Doerr [10]	Huang [4]	Huang [5]	This Work
Approach	SBS	EM	SBS	OE	OE	OE	MO	MO	EM
Broadband	Yes	No	Yes	Yes	Yes	Yes	No	Yes	Yes
Length (mm)	> 10	0.17	100	50	1.5	9	0.07	1.5	10
Power (mW)	50	100	5000	500	25	2000	9.6	260	1.14
IL (dB)	20	7.7	10	5.5	70	4	2.3	8	3.5
Isolation (dB)	25	15	20	12.5	3	3	32	29	20
Bandwidth (THz)	0.15	0.001	3.1	11.3	0.2	4.5	0.011	2.3	0.38
<b>Energy/bit (fJ/bit)</b>	<b>13,000</b>	<b>400,000</b>	<b>6,500</b>	<b>177</b>	<b>500</b>	<b>1780</b>	<b>3490</b>	<b>452</b>	<b>12.0</b>

Table 1: Comparison to other published on-chip isolators (EM – electro-mechanical, OE – optoelectronic, MO – magneto-optic).

make the optical dispersion curves in Fig. 1 parallel for maximize optical bandwidth. The group-velocity dispersions cause a quadratic dependence of phase-mismatch on detuning [Fig. 2(e)] which limits isolation bandwidth, and ‘bias detuning’ the acoustic wave gives a bandwidth-maximizing ripple. The phase-matched acoustic wave for this configuration has frequency  $\Omega/(2\pi) = 3.12$  GHz, effective wavelength  $2\pi/K = 1.25\mu\text{m}$ , optomechanical coupling coefficient  $\kappa = 2.66 \times 10^{-10} \text{W}^{-1/2}\text{s/m}$ , and device length  $L = 1$  cm.

The acoustic loss rate of  $1 \text{mm}^{-1}$  limits interaction length to much less than the needed 1 cm in this configuration. We add a new transducer every 1 mm, which in combination with the mechanical limitations of suspended beams leads us to split the 1 cm active length into ten 1 mm suspended beam sections. Each 1 mm active section is preceded by a  $30\mu\text{m}$  long acoustic injector to re-inject the acoustic wave and anchor the beam. For the acoustic injector we design an optical-mechanical mode multiplexer, a novel component required for this isolator design, and simulate single frequency acoustic performance in COMSOL and broadband optical performance in Lumerical FDTD. The multiplexer is depicted in Fig. 1 and uses silicon for optical guiding, silica for acoustic guiding, and silicon nitride as a mutual cladding. The multiplexer design has 5.8 dB acoustic insertion loss, 22.3 dB forwards/backwards acoustic injection asymmetry, and is optically transparent (reflection  $< -60$  dB, modal cross-talk  $< -60$  dB, insertion loss  $< 0.001$  dB). An additional acoustic insertion loss of 3 dB is predicted between the transducers and the multiplexer. This performance is sufficient to provide  $> 20$  dB of isolation.

We numerically simulate mode conversion in both the pass [Fig. 3(a)] and block [Fig. 3(b)] directions, accounting for loss and dispersion (material and geometrical). For this implementation we predict an insertion loss of 3.5 dB, an isolation of at least 20 dB over a 380 GHz bandwidth [Fig. 3(c)], and 1.14 mW of electrical drive power. The bandwidth can be further increased by minimizing group velocity dispersion using more sophisticated cross-section designs such as [8]. For comparison to other on-chip isolation approaches, we have collected some representative devices in Table 1, where we have assumed 0.25 bps/Hz spectral utilization and lasers with a 10% wall plug efficiency. Further comparison of non-resonant approaches to on-chip isolation can also be found in [23].

The proposed EMP isolators offer a self-contained photonic component with equivalent function to a passive isolator, and no magneto-optic materials. This comes at the cost of non-zero electrical power consumption, but as shown this power is expected to be extremely low relative to other relevant components. For example, energy per bit is a key metric for links in intra- and inter-chip optical communication applications [24]. The example isolator is more than an order of magnitude

more efficient in terms of energy per bit than the next-best on-chip approach without external magnets, both resonant and non-resonant. Being in the 10 fJ/bit regime in energy cost, it adds a negligible footprint to the energy budget of integrated photonic communication links, where modulators and detectors average 10s to 100s of fJ/bit efficiencies, respectively [1]. Other on-chip (no external magnet) isolation approaches add at least comparable amounts of power to the budget as current transceiver circuitry, which may scale further down to fJ/bit levels [24], and in the majority of cases dominate the power budget.

Further work is needed to experimentally validate this concept, as well as to investigate improved designs that achieve higher isolation, wider optical bandwidths above 1 THz, pure CMOS acoustic wave excitation, and shorter device lengths.

The EMP isolator can be extended to a 4-port circulator by adding a second mode multiplexer (resulting in one at either end of the non-reciprocal section). The circulator bandwidth is slightly degraded from picking up the multiplexer crosstalk twice, and would have 20 dB isolation and directivity over a 220 GHz bandwidth with 4.5 dB insertion loss.

**Funding Information** National Science Foundation Graduate Research Fellowship Grant (1144083); Packard Fellowship for Science and Engineering (2012-38222).

**Acknowledgments** We thank Kelvin Wagner for discussions.

## References

- [1] C. Sun, M. T. Wade, Y. Lee, J. S. Orcutt, L. Alloatti, M. S. Georgas, A. S. Waterman, J. M. Shainline, R. R. Avizienis, S. Lin, B. R. Moss, R. Kumar, F. Pavanello, A. H. Atabaki, H. M. Cook, A. J. Ou, J. C. Leu, Y.-H. Chen, K. Asanovic, R. J. Ram, M. A. Popović, and V. M. Stojanović, “Single-chip microprocessor that communicates directly using light,” *Nature*, vol. 528, no. 7583, pp. 534–538, 2015.
- [2] S. Ghosh, S. Keyvavinia, W. Van Roy, T. Mizumoto, G. Roelkens, and R. Baets, “Ce:YIG/silicon-on-insulator waveguide optical isolator realized by adhesive bonding,” *Optics Express*, vol. 20, no. 2, pp. 1839–1848, 2012.
- [3] B. J. Stadler and T. Mizumoto, “Integrated magneto-optical materials and isolators: a review,” *IEEE Photonics Journal*, vol. 6, no. 1, pp. 1–15, 2014.
- [4] D. Huang, P. Pintus, C. Zhang, Y. Shoji, T. Mizumoto, and J. E. Bowers, “Electrically driven and thermally tunable integrated optical isolators for silicon photonics,” *IEEE J. Sel. Top. Quantum Electron.*, vol. 22, no. 6, p. 4403408, 2016.
- [5] D. Huang, P. Pintus, Y. Shoji, P. Morton, T. Mizumoto, and J. E. Bowers, “Integrated broadband Ce:YIG/Si Mach-Zehnder optical isolators with over 100 nm tuning range,” *Optics Letters*, vol. 42, no. 23, pp. 4901–4904, 2017.
- [6] Y. Chen, M. Kibune, A. Toda, A. Hayakawa, T. Akiyama, S. Sekiguchi, H. Ebe, N. Imaizumi, T. Akahoshi, S. Akiyama, *et al.*, “A 25Gb/s hybrid integrated silicon photonic transceiver in 28nm CMOS and SOI,” in *IEEE International Solid-State Circuits Conference*, p. 402, 2015.
- [7] D. Jalas, A. Petrov, M. Eich, W. Freude, S. Fan, Z. Yu, R. Baets, M. Popović, A. Melloni, J. D. Joannopoulos, M. Vanwolleghem, C. R. Doerr, and H. Renner, “What is—and what is not—an optical isolator,” *Nature Photonics*, vol. 7, no. 8, p. 579, 2013.
- [8] C. G. Poulton, R. Pant, A. Byrnes, S. Fan, M. Steel, and B. J. Eggleton, “Design for broadband on-chip isolator using stimulated Brillouin scattering in dispersion-engineered chalcogenide waveguides,” *Optics Express*, vol. 20, no. 19, pp. 21235–21246, 2012.
- [9] E. A. Kittlaus, N. T. Otterstrom, P. Kharel, S. Gertler, and P. T. Rakich, “Nonreciprocal modulation via intermodal Brillouin scattering in a silicon waveguide,” in *CLEO: Science and Innovations*, pp. SM11–8, Optical Society of America, 2018.
- [10] C. Doerr, L. Chen, and D. Vermeulen, “Silicon photonics broadband modulation-based isolator,” *Optics Express*, vol. 22, no. 4, pp. 4493–4498, 2014.
- [11] P. Dong, “Travelling-wave Mach-Zehnder modulators functioning as optical isolators,” *Optics Express*, vol. 23, no. 8, pp. 10498–10505, 2015.
- [12] Z. Yu and S. Fan, “Complete optical isolation created by indirect interband photonic transitions,” *Nature Photonics*, vol. 3, no. 2, pp. 91–94, 2009.
- [13] H. Lira, Z. Yu, S. Fan, and M. Lipson, “Electrically driven nonreciprocity induced by interband photonic transition on a silicon chip,” *Physical Review Letters*, vol. 109, no. 3, p. 033901, 2012.
- [14] R. A. Soref and B. Bennett, “Electrooptical effects in silicon,” *IEEE Journal of Quantum Electronics*, vol. 23, no. 1, pp. 123–129, 1987.

- [15] D. B. Sohn, S. Kim, and G. Bahl, “Time-reversal symmetry breaking with acoustic pumping of nanophotonic circuits,” *Nature Photonics*, p. 1, 2018.
- [16] F. Eltes, D. Caimi, F. Fallegger, M. Sousa, E. OConnor, M. D. Rossell, B. Offrein, J. Fompeyrine, and S. Abel, “Low-loss BaTiO<sub>3</sub>–Si waveguides for nonlinear integrated photonics,” *ACS Photonics*, vol. 3, no. 9, pp. 1698–1703, 2016.
- [17] R. Marathe, B. Bahr, W. Wang, Z. Mahmood, L. Daniel, and D. Weinstein, “Resonant body transistors in IBM’s 32 nm SOI CMOS technology,” *Journal of Microelectromechanical Systems*, vol. 23, no. 3, pp. 636–650, 2014.
- [18] C. Wolff, M. J. Steel, B. J. Eggleton, and C. G. Poulton, “Stimulated Brillouin Scattering in integrated photonic waveguides: forces, scattering mechanisms and coupled mode analysis,” *Physical Review A*, vol. 92, p. 013836, 2015.
- [19] H. A. Haus, *Waves and fields in optoelectronics*. Prentice-Hall, 1984.
- [20] H. Li, S. A. Tadesse, Q. Liu, and M. Li, “Nanophotonic cavity optomechanics with propagating acoustic waves at frequencies up to 12 GHz,” *Optica*, vol. 2, no. 9, pp. 826–831, 2015.
- [21] W. Bogaerts, R. Baets, P. Dumon, V. Wiaux, S. Beckx, D. Taillaert, B. Luyssaert, J. Van Campenhout, P. Bienstman, and D. Van Thourhout, “Nanophotonic waveguides in silicon-on-insulator fabricated with CMOS technology,” *Journal of Lightwave Technology*, vol. 23, no. 1, pp. 401–412, 2005.
- [22] C. Sun, Y. Yu, M. Ye, G. Chen, and X. Zhang, “An ultra-low crosstalk and broadband two-mode (de) multiplexer based on adiabatic couplers,” *Scientific Reports*, vol. 6, 2016.
- [23] Y. Yang, C. Galland, Y. Liu, K. Tan, R. Ding, Q. Li, K. Bergman, T. Baehr-Jones, and M. Hochberg, “Experimental demonstration of broadband lorentz non-reciprocity in an integrable photonic architecture based on mach-zehnder modulators,” *Optics Express*, vol. 22, no. 14, pp. 17409–17422, 2014.
- [24] D. A. Miller, “Attojoule optoelectronics for low-energy information processing and communications,” *Journal of Lightwave Technology*, vol. 35, no. 3, pp. 346–396, 2017.